Chapter-3

Mathematical Modeling and Design of TPMS Porous Structures

3.1 Introduction

TPMS provide advantages in respect to design over traditional strut-based lattice structures such as BCC, honeycomb, etc. These are feasible in manipulating morphological characteristics of pores efficiently and consistently, as well as constructing smooth functionally gradient structures (gradient for shape or porosity) (Yoo 2014, Maskery et al. 2018). There are different methods for generating TPMS structures which include the parametric modeling, implicit function-based surface generation, image-based method, and CAD-based approach. The parametric modeling approach uses a function that transforms a planar area into a surface area. For implicit function-based modeling, surfaces can be generated by combining trigonometric functions with implicit functions of the first order of approximation. Image-based modeling is a CT-based approach in which cross-sectional images of 3D structures are used to generate 3D mesh models, which is a reverse modeling approach. A wide range of software like Mimics, Simpleware, 3D-Doctor, 3D Slicer, etc., are available commercially that can process the medical images to produce 3D models. However, Computational or CAD-based modeling work on the principle of gradually developing a basic polygon design into an optimal surface following the specific boundary conditions.

3.2 TPMS unit cell Investigation and selection criteria

Porous structures have particular geometrical characteristics, mechanical capabilities, and physical characteristics making them appropriate for a variety of applications in industrial and medical sectors. In orthopaedics, when reconstructive implants are required to restore damaged bone and infuse with the surrounding tissues, porous materials have some of the most significant uses. (Kujala et al. 2003, Mullen et al. 2009, Van der Stok et al. 2012, Van der Stok et al. 2013). A biomaterial with mechanical characteristics corresponding to those of the bone it substitutes is required in such applications. The biomaterial should also be capable of delivering therapeutic drugs, allow for good osseointegration and bone ingrowth, and be biocompatible. Owing their large porosity and substantial surface area to volume ratio, typical porous metal materials like porous titanium alloys, and hydroxyapatite-coated implants satisfy the above-mentioned criteria but have certain limitations. In contrast to bone, porous titanium implants have higher elastic characteristics (Yavari et al. 2013, Campoli et al. 2013, Greiner et al. 2005, Oh et al. 2003, Wen et al. 2002). But titanium alloys are well recognised for being both extremely biocompatible and corrosion-resistant (Long and Rack 1998). Porous titanium has also been demonstrated to promote bone regeneration and osseointegration due to the pores present but in conventional porous implant fabrication, there are usually chances of non-uniform distributions of pores which lead to non-uniform bone ingrowth and integration (Van der Stok et al. 2012, Pilliar 1983). Furthermore, biological components like growth factors have been delivered using the enormous surface area and abundant pore space of porous materials. For these parameters, sheet based TPMS structures are best suitable among other porous structures like strut based, conventional pores, closed pores, etc. (Van der Stok et al. 2013, Jansen et al. 2005). TPMS also have shown the ability to achieve the appropriate pore size which are permeable for various biological fluids and have the ability of revascularization to form the basis of nutrient transfer at the cellular level.

Also, TPMS have shown the ability to replicate the biomorphic geometry of human bones owing to their unique morphology. So far, fabrication of these complex self-supporting TPMS structures have been realized only by the recent development of additive manufacturing technologies like Electron Beam Melting (EBM), Selective Laser Melting (SLM), and Selective Laser Sintering (SLS) (Hao et al. 2012).

Selection criteria of the unit cell for biological implants depend not only on the mechanical behavior of lattice design but also on the internal architecture of the lattice which includes pore size, porosity, and pore interconnectivity to achieve satisfactory clinical outcomes. Increased porosity of lattice facilitates the benefit of bone tissue generation but also will reduce the mechanical strength of lattice structure. Also, the pore size of porous structure has a significant role in bone tissue ingrowth. Various works of literature have claimed that optimal pore size should range from 100-700µm and porosity must be greater than 50% to obtain better bone tissue regeneration (Peng et al. 2016, Mullen et al. 2009, Zaharin et al. 2018). A very small size pore shall obstruct bone tissue ingrowth by supporting pore occlusion, while a too-large size pore shall reduce the surface area which slows down the cell adhesion and further reduces the load-bearing capacity of the implant. Thus, an optimal range of pore size and porosity > 50% are required for better cell migration, adequate mass transportation, effective surface area for cell adhesion, and maintaining mechanical stability of implant should be selected.

Thus, in this study, a family of a remarkable class of mathematically defined surfaces known as Triply Periodic Minimal Surfaces (TPMS) was employed. Four classes of TPMS which are Gyroid, Primitive, Diamond, and IWP were recruited for this study. Selection criteria for these structures are based on the relevant literature and previous research on the advantages over other porous structures and relevant gaps which are as follows:

1. Architected D, G, IWP, and P have their unique node connectivity that mimics natural bone morphology (Vijayavenkataraman et al. 2020). The incremental nodal connectivity for the D, G, IWP, and P are four-fold, three-fold, eight-fold, and six-fold (Xiaofeng et al. 2019).

2. Biological requirements such as cell attachment, ingrowth, and differentiation are not uniquely achieved from previous reports either by strut-based porous structures or by implants fabricated by conventional porosities.

3. The four structures involved in this study are highly complex. Until recently, the challenges are there to fabricate complex porous structures. Recent advancements in additive manufacturing technique helps to mitigate the challenges and makes the study feasible.

4. Energy absorption studies have shown that sheet-based structures exhibited desirable specific energy absorption values which can be the foundation for the impact tolerance when structures are used for implant fabrication. However, tuned energy absorption for implant manufacturing is lagging in previous reports.

5. The use of different porosities reported in previous works, using different materials and their densities, and fabrication techniques restrict a fair and sound comparison between examined porous structures specifically for the anatomically matched (patient-specific and location-specific) studies.

6. Owing to the large pores in TPMS within a confined space, compared to other types of porous structures, it offers an advantage for the implants to be highly light weight specifically advantageous when fabricated for treating critical-size defects.

3.3 Modelling approaches of TPMS

Galusha demonstrated the presence of minimal surface morphologies in living tissues like beetle shells and weevils using imaging technologies, many decades back (Galusha et al. 2008, Galusha et al. 2010). Kapfer further claimed how TPMS-based sheet solids might give reasonably higher stiffness with increased porosity, allowing for the development of structural scaffolds employing TPMS (Kapfer et al. 2011To provide nutrition to the proliferating cells, Rajagopalan later created fully consistent seed-feed systems depending on Schwartz Primitive (P) surfaces (Rajagopalan and Robb 2006). By including a linear term for the z-value of Cartesian coordinate system, Melchels et al. generated the diamond (D) and gyroid (G) TPMS structures using CAD software (Melchels et al. 2010). Yoo summarised and provided a thorough CAD porous scaffold conceptual framework employing TPMS models consisting of different unit cells depending on proposed structure employing a specific TPMS in simple cube (Yoo 2011).

There are different strategies to model TPMS scaffold structure (Figure 3.1) which include: analytical and finite element based methods.

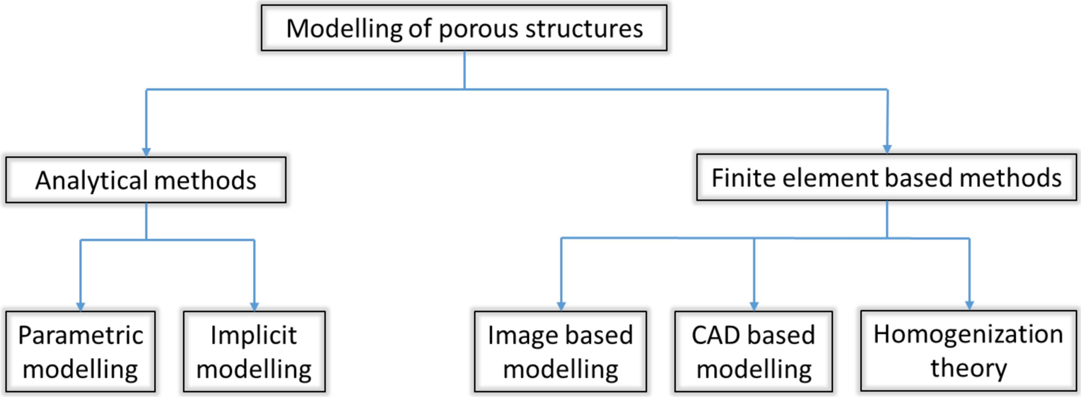

Figure 3.1: General methods for modeling porous structures.

3.3.1 Analytical methods: include parametric and implicit-based modeling approaches that use mathematical functions and trigonometric equations.

Parametric modeling: This approach uses a function that transforms a planar area into a surface area. It uses Enneper-Weierstrass representation where nodal coordinates of the TPMS surface are evaluated to determine the integral function of the Weierstrass equation (Gandy et al. 2001). It is discussed in detail in the next section.

Implicit-based modeling: In this method, the TPMS surface represents the scalar-valued functions of three independent variables which represent those surfaces that are composed of a trigonometric function. Table 3.1 shows a list of commonly used TPMS surfaces with their trigonometric functions reported in the literature (Yoo 2011).

Table 3.1: Nodal equations of some commonly used TPMS structures (Yoo 2011)

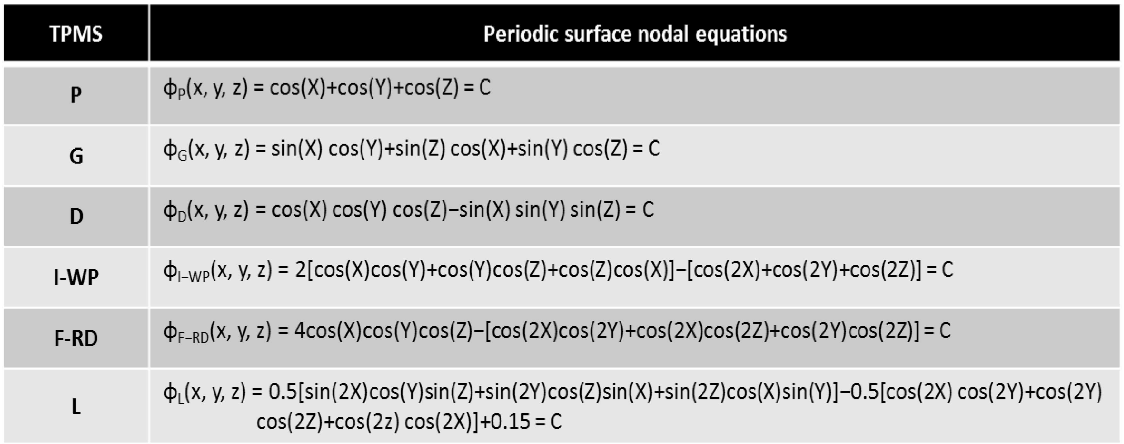

TPMS	Periodic surface nodal equations
P	$\phi_P(x, y, z) = \cos(X)+\cos(Y)+\cos(Z) = C$
G	$\phi_G(x, y, z) = \sin(X)\cos(Y)+\sin(Z)\cos(X)+\sin(Y)\cos(Z) = C$
D	$\phi_D(x, y, z) = \cos(X)\cos(Y)\cos(Z)-\sin(X)\sin(Y)\sin(Z) = C$
I-WP	$\phi_{I-WP}(x, y, z) = 2[\cos(X)\cos(Y)+\cos(Y)\cos(Z)+\cos(Z)\cos(X)]-[\cos(2X)+\cos(2Y)+\cos(2Z)] = C$
F-RD	$\phi_{F-RD}(x, y, z) = 4\cos(X)\cos(Y)\cos(Z)-[\cos(2X)\cos(2Y)+\cos(2X)\cos(2Z)+\cos(2Y)\cos(2Z)] = C$
L	$\phi_L(x, y, z) = 0.5[\sin(2X)\cos(Y)\sin(Z)+\sin(2Y)\cos(Z)\sin(X)+\sin(2Z)\cos(X)\sin(Y)]-0.5[\cos(2X)\cos(2Y)+\cos(2Y)\cos(2Z)+\cos(2z)\cos(2X)]+0.15 = C$

Where $X = 2\pi x$, $Y = 2\pi y$, $Z = 2\pi z$. C denotes level set constant that defines gradient in sizes and volume fractions of pore.

3.3.2 Finite element-based methods: include CT-based modeling, CAD-based modeling, and homogenization methods.

CT-based modeling: It is an image-based modeling approach in which 3D images of structures are used to generate 3D mesh models. It is a reverse modeling approach. A wide range of software like Mimics, Simpleware, 3D-Doctor, etc., are available commercially that can process the medical images to produce 3D models.

Computational or CAD-based modeling: It works on the principle of gradually developing a basic polygon design into an optimal surface following specific boundary conditions. This method comprises the following steps used to create TPMS structures:

- In this method, a polygonal surface (based on the desired TPMS surface) is defined under a boundary that is continuously optimized to reduce the surface of a polygon that spans within the boundary. A plane is created to maintain the efficiency of optimization. The spanned surface is repeatedly adjusted using the plane inside the defined boundary until any of its nodes or edges can be shifted to minimize the area. This produces one surface of a unit cell.

- This surface is then angularly arranged in different three-dimensional directions to obtain a complete unit cell structure.
- The unit cell is scaled and patterned in three Cartesian planes (x, y, and z) to obtain the cubic sheet solid structure of TPMS.
- Further, these sheet-based TPMS structures can be assigned with varying thicknesses to obtain desirable porosity.

Homogenization theory: It employs a multi-level approach, with the macro-level model serving as a homogeneous model of the entire structure, whereas the micro-level model accurately depicts the micro-architecture of the structure.

However, understanding the advantages and disadantages of the above-mentioned approaches, a dual approach is adopted in this research work to design and develop TPMS-based lattice structures, which includes: the analytical method (Implicit-based modeling) followed by a CAD-based modeling strategy (Figure 3.2). Initially, the implicit-based modeling approach is used to generate TPMS structures that are sufficient for AM, whereas for finite element analysis we have adopted a CAD-based modeling approach.

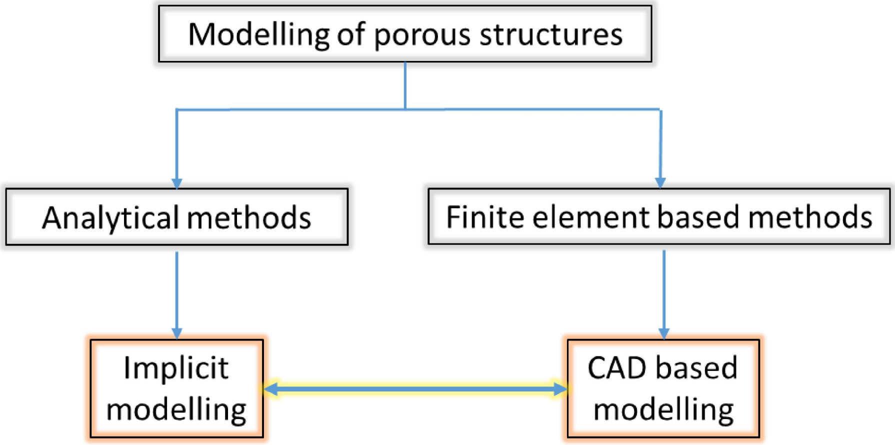

Figure 3.2: Dual approach for modeling TPMS structures.

3.4 Mathematical representation of TPMS

3.4.1 Parameterization of TPMS structures

Parameterization allows reconstructing the minimal surfaces of TPMS structures and straight reconstruction of curvatures and normals. The Weierstrass representation uses a Gaussian map and stereographic projection to produce robust parameterization.

3.4.1.1 The Gauss map

The Gauss map maps a surface to the unit sphere. Let $\underset{n}{\rightarrow}\underset{(p)}{\longrightarrow}$ be the unit normal at a point $\underset{p}{\rightarrow}$ on the surface. The position vector of the image of a point $\underset{p_0}{\rightarrow}$ on the surface is then given by $\underset{n}{\rightarrow}\underset{(p_0)}{\longrightarrow}$. In other words, each point on the surface is mapped to the unit sphere via its unit normal (Figure 3.3).

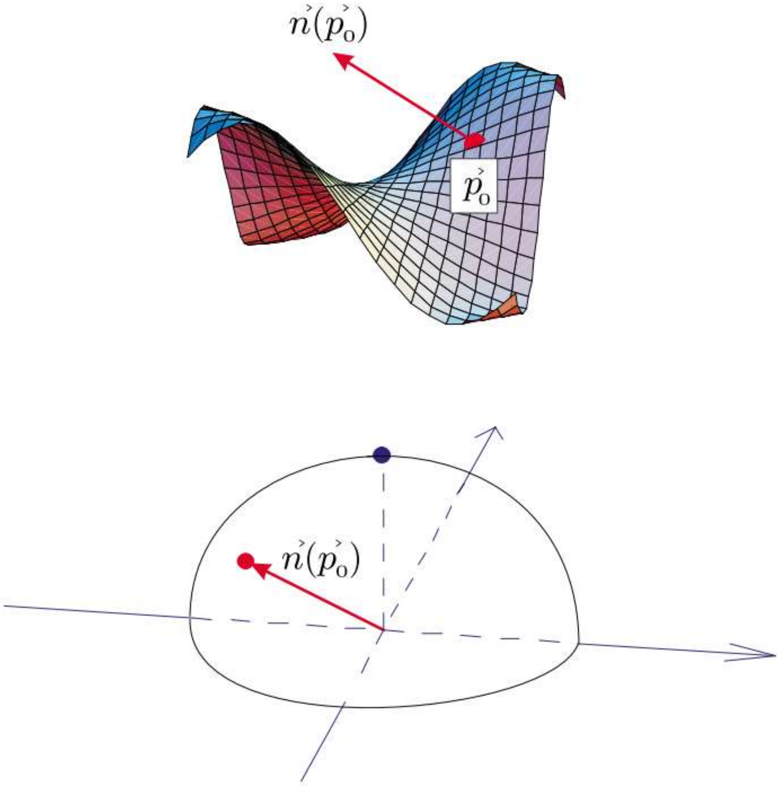

Figure 3.3: Representation of Gaussian map.

3.4.1.2 Stereographic Projection

A stereographic projection maps points on the unit sphere to a plane. The image point is determined by the intersection with the plane of the line through the point under consideration and the "north pole" of the sphere (i.e. the point with coordinates (0, 0, 1) as shown in Figure 3.4.

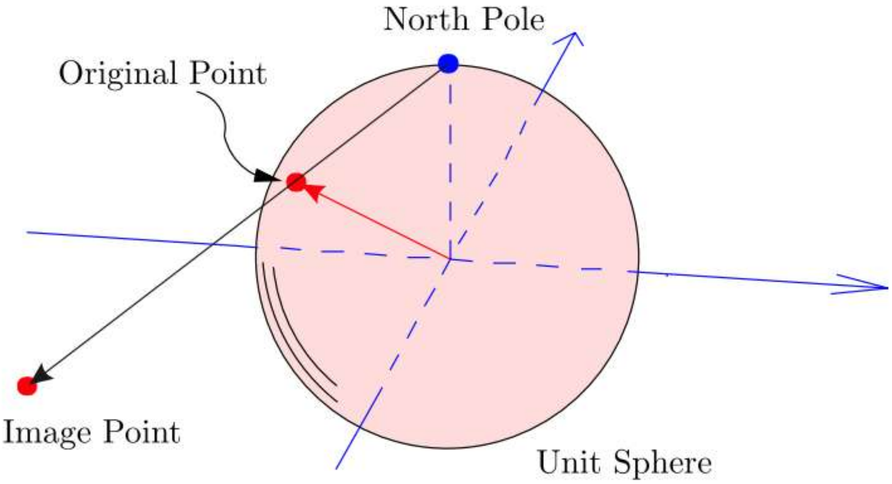

Figure 3.4: The Weierstrass representation and Bonnet transformation.

The Weierstraß representation shows an inverse mapping of the composition of the Gauss map followed by a stereographic projection. The minimal surface coordinates of TPMS are expressed by using Enneper-Weierstrass representation parametrically, in which nodal coordinates of the TPMS analytical surface may be calculated by computing the integral function of the Weierstrass equation (Gandy et al. 2001). They are represented by the Equation 3.1 as follows:

$$\begin{aligned} x&=\mathrm{Re}\left(e^{i\theta}\int_{\omega o}^{\omega}(1-\tau^2)\,R(\tau)\,d\tau\right)\\ y&=\mathrm{Re}\left(e^{i\theta}\int_{\omega o}^{\omega}i(1+\tau^2)\,R(\tau)\,d\tau\right)\\ z&=\mathrm{Re}\left(e^{i\theta}\int_{\omega o}^{\omega}2\tau R(\tau)\,d\tau\right)\end{aligned}\tag{3.1}$$

Where; $i^2 = -1$, θ is the bonnet angle, τ represents a complex variable ($\tau= \tau_a+ i\tau_b$), and $R(\tau)$ represents the Weierstauss function, which changes depending on the surface. The integration of the Weierstauss function determines a minimal surface design. Although, the integrals can be numerically calculated by integrating, but till now have been assessed analytically for some specific surfaces. It is possible to develop a complete set of different minimal surfaces from the same metrics and Gaussian curves with the help of Bonnet transformations in the form of a Bonnet angle. By changing θ, several associated surfaces can be developed. For example, for θ = π/2, the associated surface transforms into a conjugate surface. For the D surface, θ = π/2 (90°) for the P surface, and G surface, θ = 38.0147°.

Since the Weierstauss function R(τ) exceptionally influences TPMS characteristics, it is known to exist only for limited TPMS surfaces with simplest configurations like P, G, and D (Cvijovic´and Klinowski 1992, Cvijovic´and Klinowski 1993, Cvijovic´and Klinowski 1994, Gandy et al. 1999) . Therefore, R(τ) can be formulated only if a basic patch (flake) of concerned TPMS is available that enables the development of a complete TPMS unit cell surface by either mirroring or rotating the patch symmetrically (Cvijovic´and Klinowski 1992).

For the P, D, G surfaces of TPMS family, R(τ) can be formulated as Equation 3.2:

$$R\ (\tau)=\frac{1}{\sqrt{1+\lambda\tau^4+\tau^8}} \tag{3.2}$$

Where λ = - 14. Generally, R(τ) is governed by the values of τ showing planar curvatures having a mean of zero on the minimal surfaces expressed as $\pi_i(\tau-\tau_i)^\eta$ where η represents the surface topology.

3.4.2 Mathematical equations of TPMS

TPMS of particular interest, in this work, are the D, P, G, and IWP minimal surfaces. These surfaces share a bicontinuous nature with the experimental liquid crystal center surfaces, which are cubic (i.e. have cubic unit cells), and have the desired symmetries. Compared with the above parametrized TPMS, the method can only generate a few different types of TPMS. In a more general way, TPMS are approximately defined by the combination of trigonometric functions. So, the P, D, G, and IWP surfaces can be generated by combining trigonometric functions with implicit functions of the first order of approximation as expressed in Equations 3.3 – 3.6 (Guo et al. 2019, Verma et al 2020, Vijayavenkataraman et al. 2018):

F (Diamond): $cosXcosYcosZ - sinXsinYsinZ = c$ (3.3)

F (Gyroid): $sinXcosY + sinYcosZ + sinZcosX = c$ (3.4)

F (IWP): $2((cosXcosY + cosYcosZ + cosZcosX) - (cos2X + cos2Y + cos2Z)) = c$ (3.5)

F (Primitive): $cosX + cosY + cosZ = c$ (3.6)

3.4.3 Surface Triangulation of TPMS

For computational convenience, the minimal surfaces (also known as isosurface) is approximated with a mesh of planar triangles. The Weierstraß equations can be used to generate a set of points lying on a patch of each surface, which can then be triangulated using a Delaunay algorithm. As the patch is reproduced, rotated, and translated to construct the surface and the vertices are merged where appropriate. Careful choice of the initial set of points allows vertices on the patch edge to line up with those from adjacent patches, minimizing merging difficulties. For this, an efficient algorithm is developed in Matlab which utilizes a marching cube (MC) algorithm, for each TPMS structure separately (Appendix). The fundamental concept behind this approach is to approximate the implicit surface with a new minimal surface by connecting the intersection points of the minimal and hexahedron edge in a specific manner. Figure 3.5 depicts the Marching Cubes algorithm flowchart.

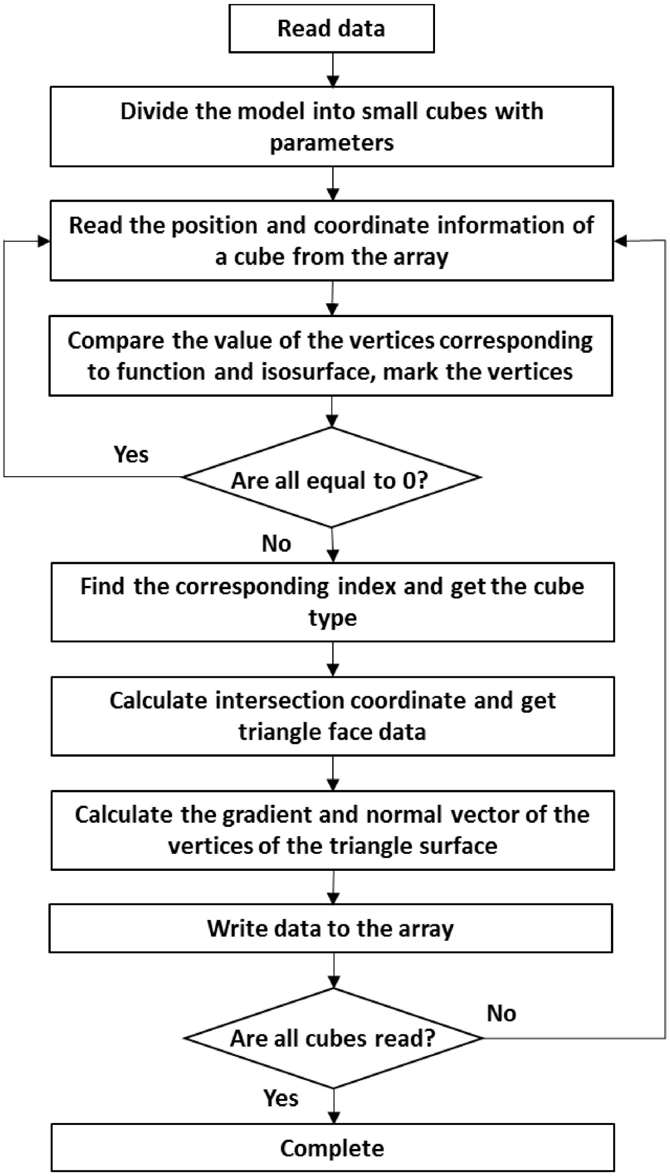

Figure 3.5: Flowchart illustrating the Marching Cubes algorithm.

The Marching Cubes approach is advantageous because to its simple algorithm and efficient computation time. Though certain triangle patches with extremely tiny or wide angles will be formed due to the inability to manage the angles of triangle patches, this results low qualities of triangle patches, that makes them unsuitable for the development of tetrahedral mesh during FEA. Therefore, an efficient approach of optimization for the elimination of the aforementioned issues in addition to the other issues has been developed which are discussed in detail in a later section. A sample of the coarsest of the triangulations used is shown in Figure 3.6, together with the resulting shaded image.

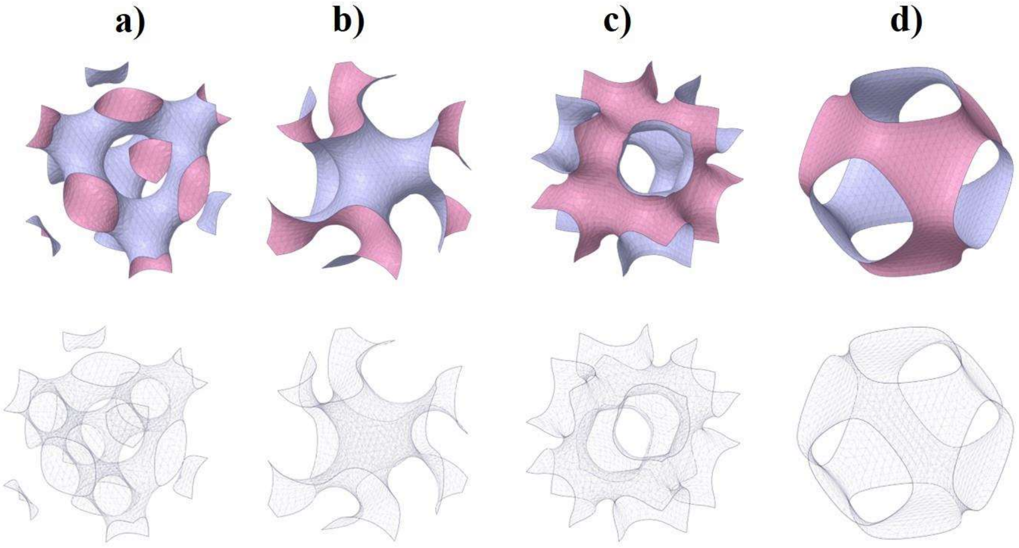

Figure 3.6: Surface triangulation of a) Diamond b) Gyroid c) IWP and d) P structures.

3.4.4 Bilayer surface generation

Sheet-based structures are triangulated and discussed in the above section. However, to obtain the thickness of the above TPMS structures it is important to evaluate the bilayer surfaces of the above triangulation. Due to the symmetric nature of TPMS structures, the second surface will be approximately parallel to the outer surface and is generated by translating each point on a surface at a constant distance along the normal vector to the surface at that point as shown in Figure 3.7.

A standard differential geometry result (Nackman, 1982) relates the Gaussian and mean curvatures (denoted by K and H, respectively) of a surface Y that is parallel to X:

$$K_Y = \frac{K_X}{1 - 2cH_X + c^2K_X}$$

$$H_Y = \frac{H_X - cK_X}{1 - 2cH_X + c^2K_X}$$

A representation of surface Y parallel to surface X is illustrated in Figure 3.7 for the gyroid surface which is generated by the code developed in MATLAB (Appendix).

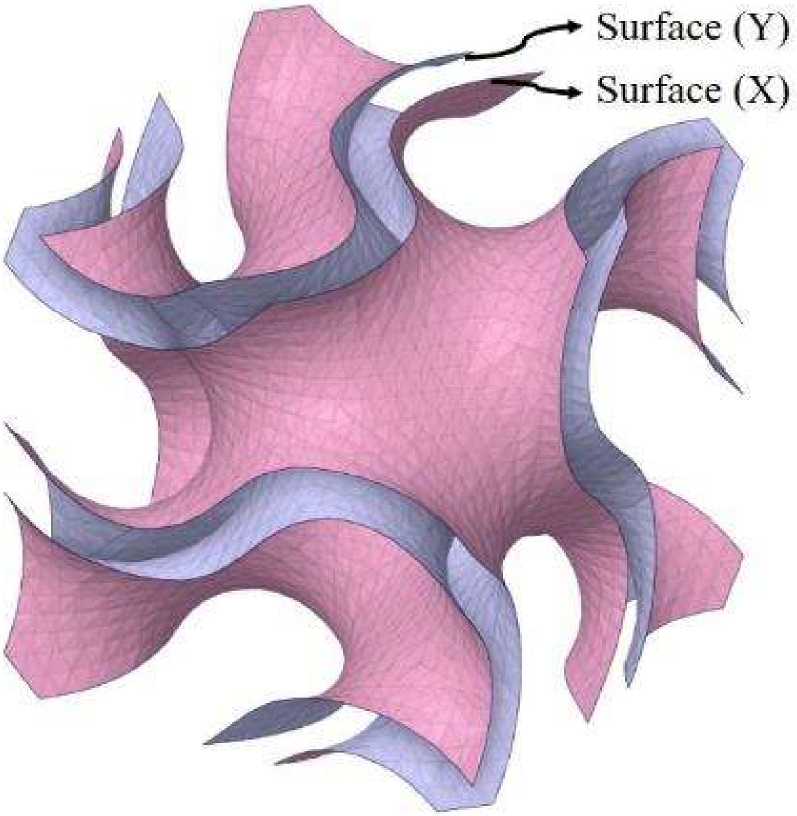

Figure 3.7: Parallel surfaces centered on a unit cell of the gyroid minimal surface.

3.4.5 Capping parallel layers

For the parallel surface of TPMS, generated by the marching cube algorithm, it is important to close the open ends to form a thickened (closed) TPMS structure. A plane consisting of triangles is fitted to the open ends of both the parallel implicit surfaces. For this, ISOCAPS function is used which closes both the open ends, an illustration is shown in Figure 3.8.

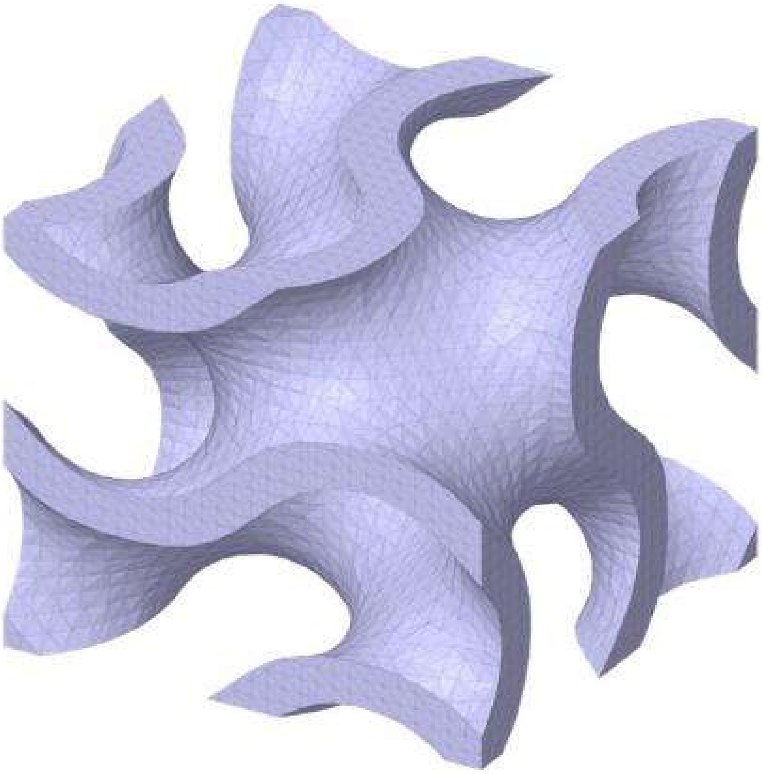

Figure 3.8: Illustration of triangulated closed implicit surfaces for the gyroid structure.

All the codes were written in Matlab for the generation of implicit surface, bilayering, and capping to obtain a complete unit cell for all four structures of TPMS.

The STL model (stereolithography) is readily generated when the implicit surfaces are recovered using the Marching Cube technique, so the STL model has the triangular features of exterior surface of models.

3.5 Code implementation and TPMS UNIT CELL Generation

The unit cell is designed with MATLAB code with the use of trigonometric equations mentioned in section 4.4.2 of the corresponding TPMS structures where, x, y, and z are the coordinates and $X = \frac{2\pi Nx}{L}, Y = \frac{2\pi Ny}{L}, Z = \frac{2\pi Nz}{L}$ where; *N* is the number of unit cells; L defines the length of the unit cell and parameter ‘c’ controls the volume of the surface.

3.5.1 Role of level set constant ‘c’

The effect of varying a level set parameter ‘c’ in trigonometric TPMS mathematical equation has been studied and found that level set parameter determines volume fraction and is used to control the position of the boundary between solid and void in TPMS structure (Al-Ketan and Abu Al-Rub 2021, Li et al. 2019). If the value of c is zero, the obtained minimal surface divides the region into sub-regions of equal volume. The thickness varies as the magnitude of level constant (c) is increased or decreased, therefore, it is an essential parameter used as a control constraint. Once the level constant, (c), is zero, the TPMS surface is completely minimised. The mean curvature at each point on the surface approaches zero in this scenario, implying that the surface could not be generated. To obtain the surface of TPMS, the level set constant must be a non-zero quantity as can be seen in Figure 3.9 for all the four TPMS structures, none of the curves coincides at zero. When c has a non-zero value, the mean curvature changes from zero to non-zero but stays constant throughout the surface, and a volume fraction is produced. However, when the level set constant is made lower or higher than a certain value, for the respective structures, the continuity of the surface is lost. From Figure 4.9, it can be observed that for all the four structures the level is approximately varying between the ranges of -3 to +3. Surprisingly, between these ranges, all the volume fractions can be obtained. The maximum and minimum range values beyond which we obtain the disconnections of the surface are mentioned in Figure 3.10 and are also illustrated.

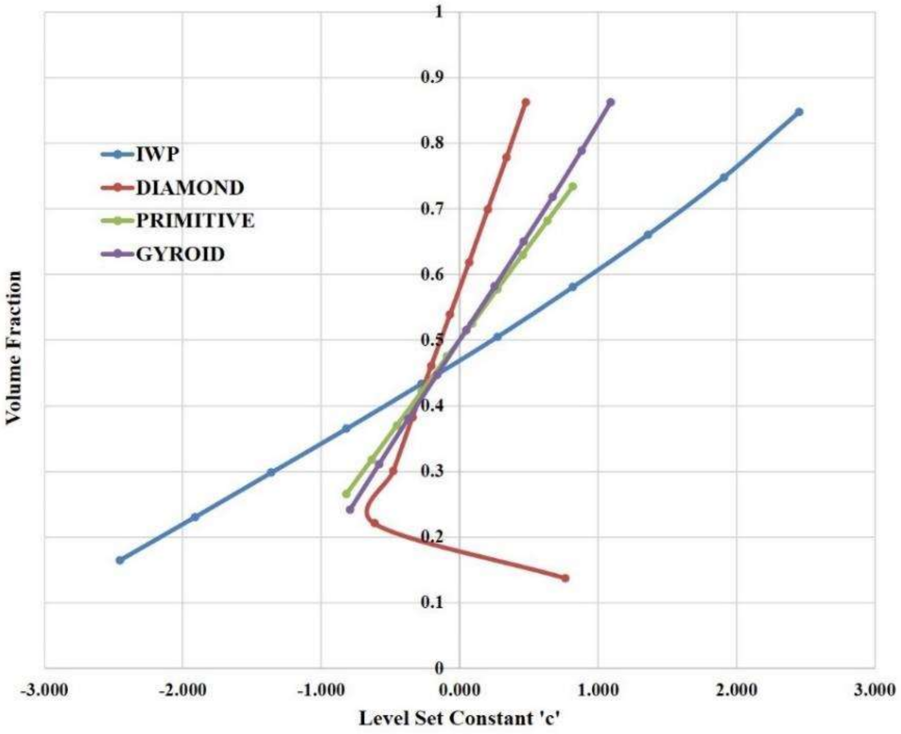

Figure 3.9: Relation between volume fraction and the level set constant ‘c’.

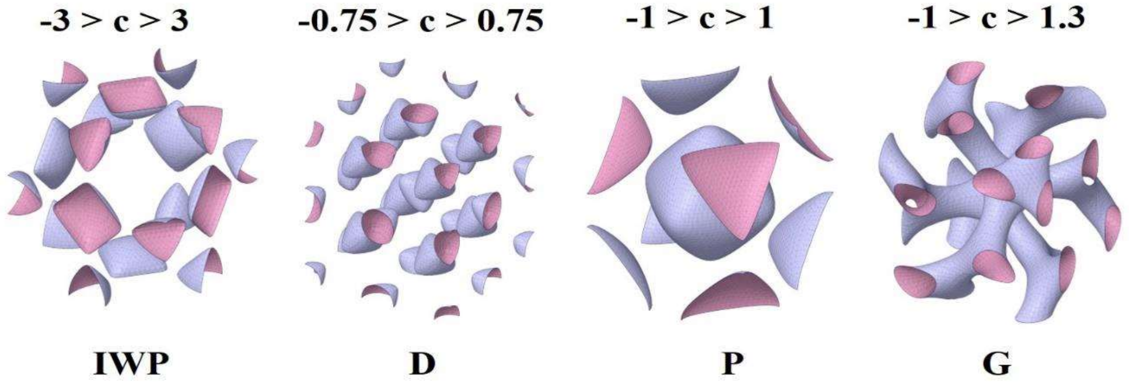

Figure 3.10: Disconnections of the implicit surface and their corresponding ranges.

Within the range of ‘c’ where continuous structures are obtained, a higher-order polynomial fit can be done on the results to better represent a relationship between level set parameter and volume fraction.

The volume fractions included in this study and their corresponding level set constants are tabulated in Table 3.2.

Table 3.2: Calculated level set constants for the volume fraction ranging from 50% to 10%.

Volume fraction (%)	Level set constant 'c'			
	IWP	**Diamond**	**Primitive**	**Gyroid**
50	±1.85	±0.43	±0.873	±0.7664
40	±1.5/1.5	±0.35	±0.7	±0.6172
30	±1.15	±0.27	±0.527	±0.468
20	±0.8	±0.19	±0.4	±0.3188
10	±0.45	±0.1	±0.19	±0.1696

3.5.2 UNIT Cell generation

TPMS isosurfaces of all the four unit cells were generated using MATLAB code. The marching cubes (MC) algorithm is implemented, which directly calculates the coordinates of the point in a 3D data field on the surface, using a previously determined level constant (c) (Yoo 2011). The intersecting points, as well as hexahedral sides of the isosurface, are linked together specifically in the MC approach, and the resulting isosurface has been approximated such that it reveals the implicit surface. ISOSURFACE command determines isosurface by connecting points of a constant value within a volume of space and ISOCAPS determines isosurface end-cap geometry for the volume data at specified isosurface value as discussed in the previous section. Corresponding unit cells of 1×1×1 are obtained by putting the unit value of L, which is described as the length of a unit cell, and N=1, described as the number of unit cells (mentioned above), and the output was obtained in the stereolithographic (STL) format by supplying STLWRITE command. Obtained STL templates of corresponding TPMS unit cells at this stage are directly used for manufacturing.

3.6 Optimization and modification of unit cells

Since, as specified in section 3.4.3, the angles of triangular patches are uncontrollable by the use of the marching cube algorithm, these obtained structures are inappropriate for solid conversion or the generation of triangular meshes when directly employed for FEA. To improve the quality of triangles, numerous processes are involved, which are detailed in this section, and form the basis of an efficient strategy for high-quality TPMS unit cell generation.

The obtained 3D model of structures in STL format contains errors in the form of holes, overlapping triangles, inverted normal, bad edges, etc., which is shown in Figure 3.11 that may affect its performance when directly used without optimization. The obtained error may be one or more than in one single generation. Hence, these errors must be removed or reduced as much as possible. This can be done by many software utility tools. In this work, we have used FreeCAD open-source software, and the facets module of SPACECLAIM software supplied by ANSYS.

However, using algorithm additional parts can also be generated which may be a part of the structure or generated by algorithm limitations. Lastly, upon the removal of certain errors mentioned above, polygonal mesh refinement is done using regularization tool to obtain uniform triangles with appropriate equilateral triangles by careful consideration of preserving geometrical features. The manual edit required for refining is particularly time consuming since it frequently entails erasing each intersected and overlapped triangle or the errors seen in the image below. These regions must then be made regular by adding triangles, and they must closely reflect the initial geometric features. Because of this, they are vulnerable to user error. These are vital steps to create a better mesh, but they cannot be ignored even though their incidence may be decreased with appropriate automated specifications. The facet refinement will enable smooth facets representing a smooth surface structure. Finally, an optimized model is obtained that are appropriate for conversion into solid model.

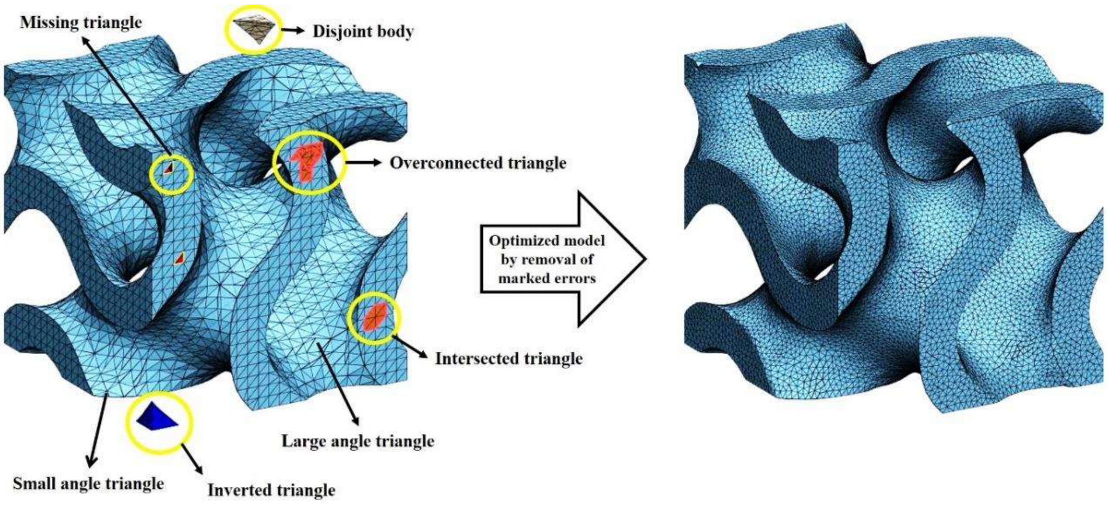

Figure 3.11: Illustration of possible errors in the use of marching cube algorithm.

3.7 Conversion of STL unit cell to the solid model

Obtained optimized STL model of unit cells as divide the surface into a sequence of triangles, where each face of the triangle represents an area of the object's outer surface. STL formats are of two types namely, the ASCII (American Standard Code for Information Interchange) and Binary.

Since STL models are tessellated triangular (faceted) meshes that employ points and edges to construct spatial triangles to approximate the 3D surface (entirely hollow inside) and cannot be modified, they are not suitable for finite element analysis (FEA) as they do not have any CAD model attributes such as virtual solid volume. However, due to the fundamental difference between surface mesh and 3D finite element mesh, STL data cannot be directly utilized in FEA. It is necessary to transform the STL into a solid body that preserves the overall surface and volume data information to employ 3D elements such as tetrahedral or hexahedral elements.

Nevertheless, a variety of methods for developing conceptual solid models are reported in the literature (Mortenson 1997), and they may be divided into two primary categories: boundary representation (BRep), that describes the surface between solid and its surroundings, and volume representation (VRep), that describes entire solid point by point (Figure 3.12). BRep methods are classified into two types: discrete (the surface is defined by a polygon mesh) and continuous (the surface is represented by a mathematical equation). When transmitting data using the.stl or.ply file format, surface triangles are frequently used in visualizing, modeling, reverse engineering, sculpting, and CAD/CAM. On the other hand, the last 60 years have seen the emergence of mathematical definitions of surfaces, that are the basis of computer-aided 3d modelling, such as Bernstein polynomials (Bernstein 1912), Bézier surface (Bezier 1966, Bezier 1967, Bezier 1970), B-Spline, NURBS (Piegl and Tiller 1997) and subdivision algorithms (Catmull and Clark 1978, Doo and Sabin 1978). These methods focus primarily on freeform surface modelling for a variety of industries, including biomedicine, automobile, shipbuilding, aircraft, and product engineering, etc.

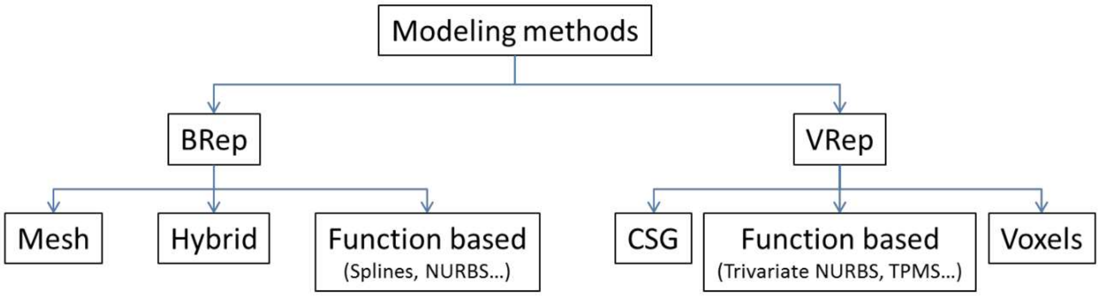

Figure 3.12: Methods for generating solid geometries

Complex solids are defined as elementary geometry's Boolean operations (union, intersection, and subtraction) in the Constructive Solid Geometry (CSG) scheme, which finds its principal use in the geometric modelling of mechanical systems (Mortenson 1997). When doing a finite element analysis to speed up the data pre - processing phase (Cottrell et al. 2009), or when warping 3D models, a solid may also be characterised point-by-point by using function-based techniques like parameterized solids or trivariate NURBS. Discrete techniques are used in solid representation, as in surface description. For instance, voxel-based (volumetric picture element) method is used to reconstruct 3D medical image from magnetic resonance imaging and computed tomography . The more advanced octrees, which are dependent on the recursive subdivision of a cube element, are the progression of this concept (Mortenson 1997). Such approaches must be modified to be acceptable in large structural geometric modelling because of large number of elements, complex shapes, and multi-scale properties. Additionally, even though with increasing interest in additive manufacturing in recent years, the ability of commercialized CAD software to model products manufactured with porous architectures is quite limited (Thompson et al. 2016).

Wang et al. devised a dual geometric modelling approach for minimal surface based porous structures using ACIS (Corney 1997) as the geometrical modelling kernel (Wang et al. 2005). This approach developes an STL model for every structure and then combines them to create the entire structure rather than modelling the entire structure in BReps and thereafter exporting it to STL. This enables for faster calculation. To smooth the geometry and prevent non-manifold geometry, they later added a spheres to every node. Chen created a general framework based on Wang's results, where the structural configurations are described in an XML file that contains all the types and data of nodes and struts (Chen 1997). After that, the XML file is transferred into a system that generates mesh-based structures. Additionally, a filleting operation is carried out, in which the fillets are represented by combining two offset operations (Rossignac, J.R., and Requicha, 1986) and applying the Minkowski summation and differences of two sets (Hadwiger 1950). The technique is however enhanced (Chen 2007) with the use of a space warping method to meet design specifications like constructing structure with small and thick cells when required. Following the development of the structure with the

XML files, the space warping is done by reducing an energy function. The ability to generate internal porous structures inside a conventional design domain is also provided.

To construct periodic porous geometries, Savio et al. suggested a modelling and optimization approach, in which an optimum model was developed to achieve the required usage for every element (Savio et al. 2015). Then, the spherinder (a cylinder with spherical caps) (Eusebeia 2017), is used to model the optimal geometric model, moving around every line of the wire model (BReps). A novel technique is suggested (Savio et al. 2016) for such single cube cell types after analysis of several cell types. This technique eliminates NURBS modelling by employing a mesh model that has been sequentially smoothed utilising Catmull-Clark subdivision method (Catmull and Clark 1978), that lowers stress concentrations and lengthens durability. Then, a generalisation of the mesh approach to work with various types of cells is described, addressing major problems with complicated models addressed in the literature, including scaling, robust behaviour, and automating (Savio et al. 2018).

In light of these issues and limitations of particular CAD packages, an efficient method for converting STL to a solid body is proposed in this section which uses BRep continuous function-based NURBS approach to represent the approximate surfaces of STL, offering simple applications, minimal processing resource and substantial memory requirements, durability, an efficient approach to get fillets, and appropriate data transfer formats.

3.7.1 Brief introduction to NURBS surface generation

The Bézier curve, which is scaled above a total of different control points, defines the NURBS surface concept (Roger, 2001). In order to construct a single continuous surface that represents a greater region, a single arc therefore accounts for several unaligned control points produced by the errors (Figure 3.13). The ideal way to merge NURBS modelling with FE modelling is to utilise a continuous, effective, semi-automated resurface methodology by removing maximum of the geometrical errors after segmentation.

The NURBS surfaces will not only remove the sharp edges and provide a smoother geometric features, but the resurface process will also need less FEs for the meshes. The amount of FEs in a voxel may consequently reduce while their size may increase because the dimensions of the reconstructed surface would expand (Figure 3.14). By eliminating the voxel-based surface generated by the sharp edges of the model and reducing the overall amount of surfaces, NURBS resurfaces the whole model. The estimated computational processing time may presumably be reduced and converged at a considerably rapid rates if the mesh included fewer FEs.

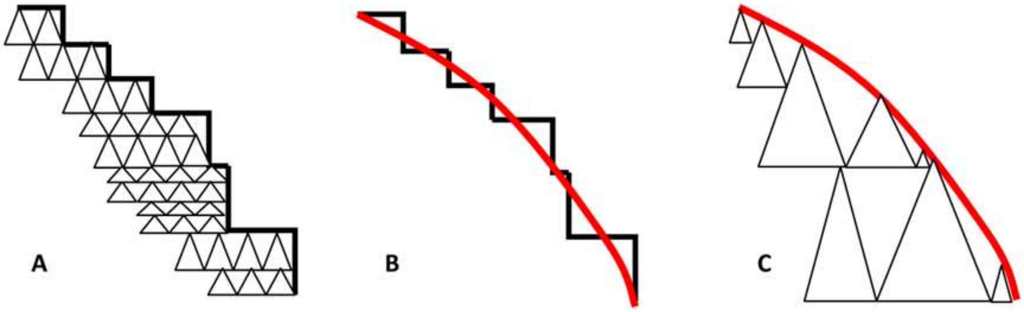

Figure 3.13: NURBS resurfacing process for isolated regions of artefact. (A) Sharp edges are visible on the surface of segmented structures (black outlines) (B) NURBS (red curve) resurfaces the edges by integrating the control points. (C) The volumetric FEs are reduced by smooth surfaces.

The challenge throughout the resurfacing procedure is whether the surface consistency will be maintained. The TPMS structure will have to maintain the distinguishing features and depict accurate structural elements suggested by STL models as the objective of smooth surface is to reduce the geometrical errors and provide a compatible FEM. The TPMS structure must also have minimal uncertainties that is within a particular threshold of variation.

3.7.2 Freeform resurfacing of TPMS unit cells

To develop appropriate FEMs from optimised STL models (as explained in the previous section), the models must be resurfaced to avoid geometrical errors and minimize the level of surface polygon. It would need fewer FEs for each surface and less computational burden since bigger resurfaced boundaries would be incorporated into the smooth contours.

To execute the process of resurface in SPACECLAIM, “Autoskin” tool was used. Each STL unit cell involved in this study was imported and resurfacing was performed individually. The STL file was opened step by step in SPACECLAIM in the form of a “facet”. At this stage, one issue arises due to the use of CAPPED STL models i.e, the right triangle edges at the boundary were sharper having an angle above 120°, which restricts the autoskin tools (Figure 3.14 left). To reduce the angle below 120°, the geometrical features of the unit cells were lost at the boundary (Figure 3.14 right).

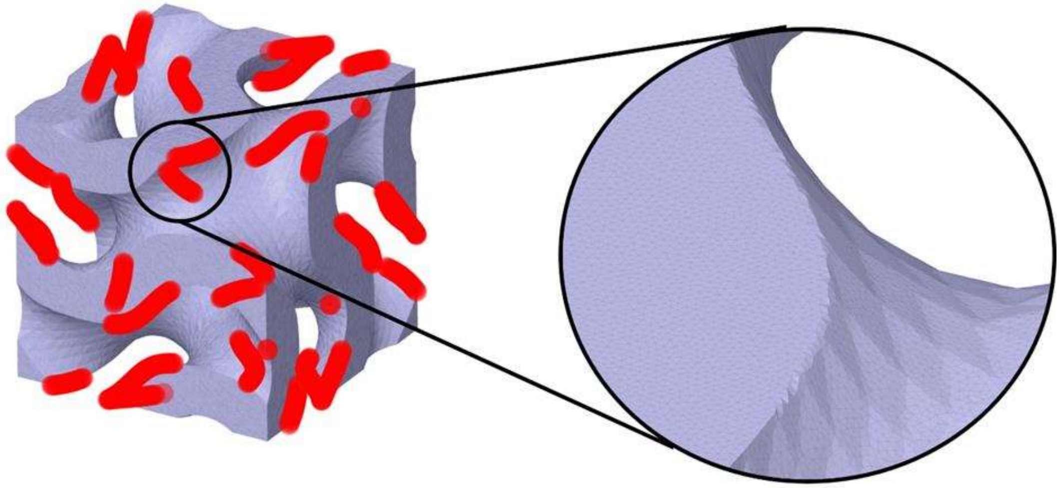

Sharper boundary edges
angle greater than 120°

Eliminating sharper edges
defeatures the boundary

Figure 3.14: Illustration of issues using CAPPED STL models

Hence, to preserve the features of the original geometry we can reduce the triangle edge length to an extent, where the surrounding sharp edged triangles have the smaller angles, which will accurately capture curvatures in NURBS fitting, but this method was not used because of computer hardware limitations.

To overcome this issue, an efficient technique is employed in this work by importing both the parallel nonintersecting surfaces in STL format without capping (open parallel surface), and optimized to the extent with curvature preserving features, as discussed in previous section, which ensures that the curvature is preserved. Later, autoskin tool was applied on both the surfaces which approximately fits the NURBS patches over the STL triangulated surfaces. By this operation, surface of the unit cells are obtained. However, the solid model (watertight model) is still not achieved at this stage since, the boundary of both the surfaces is not capped but lies on single plane in all coordinates. For this, individual planes are selected and boundary is sketched by projecting curves from the edges of both the surfaces and later on surface was drawn over by 'fill' tool. In this way a solid geometry of each unit cells is obtained. A complete step-by-step process is demonstrated in Figure 3.15 to develop solid model of unit cell from non-intersecting STL surface.

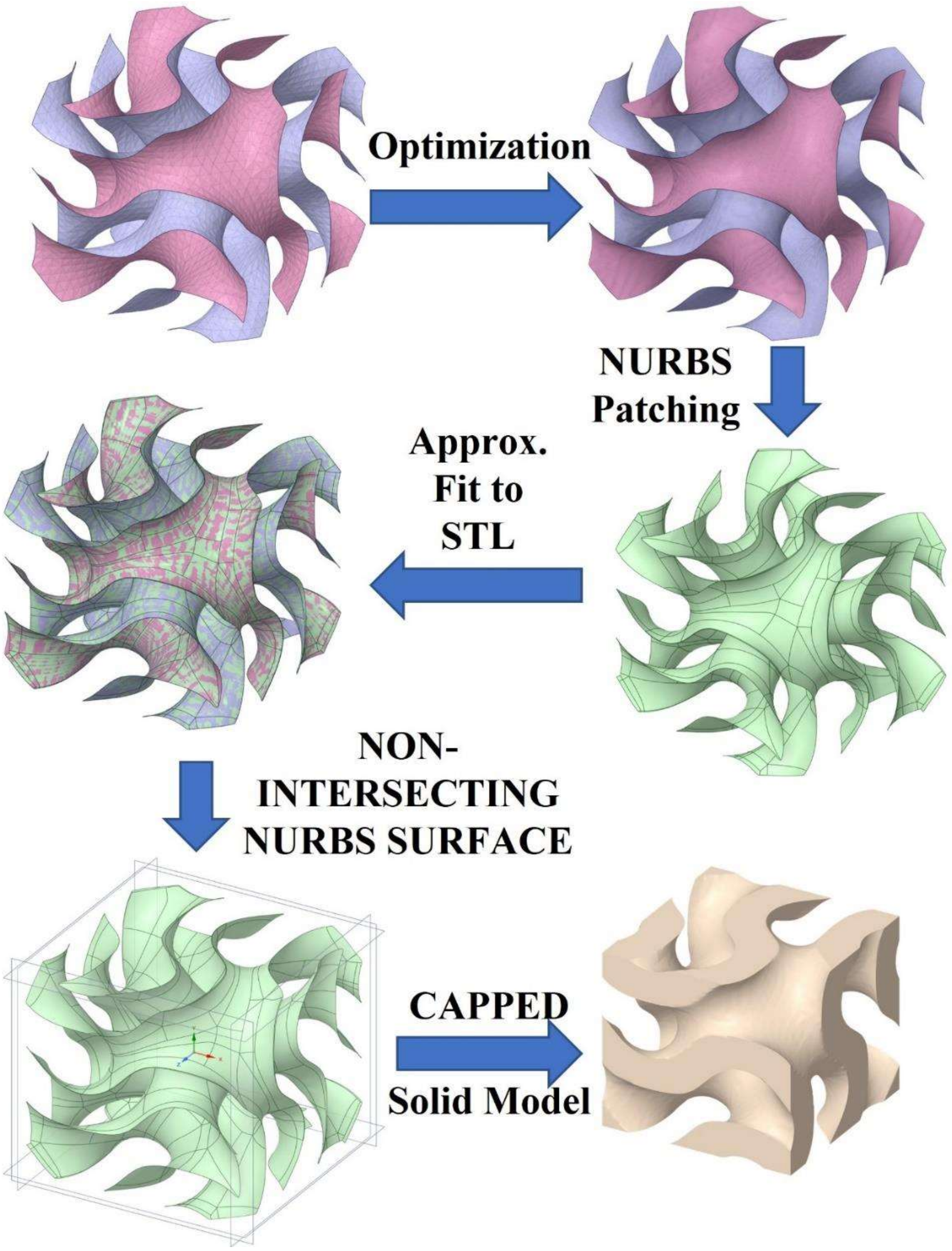

Figure 3.15: Step sequence followed to develop solid model of unit cell from non-intersecting STL surface.

Finally, in the similar fashion solid models for each of the TPMS unit cells have been extracted that are involved in this study and have the external volume shape and internal unit parameter information which can be directly used for finite element study.

The overall methodology discussed for the optimization of stl in this section is illustrated by the process flow diagram for the robust development of solid CAD models from STL (Figure

3.16). Besides, the methods discussed here are not restricted to the TPMS based unit cell conversion but, can also be used for any other STL models efficively where, two non coplaner non intersecting isosurfaces are present and have the external boundary laying on any single plane.

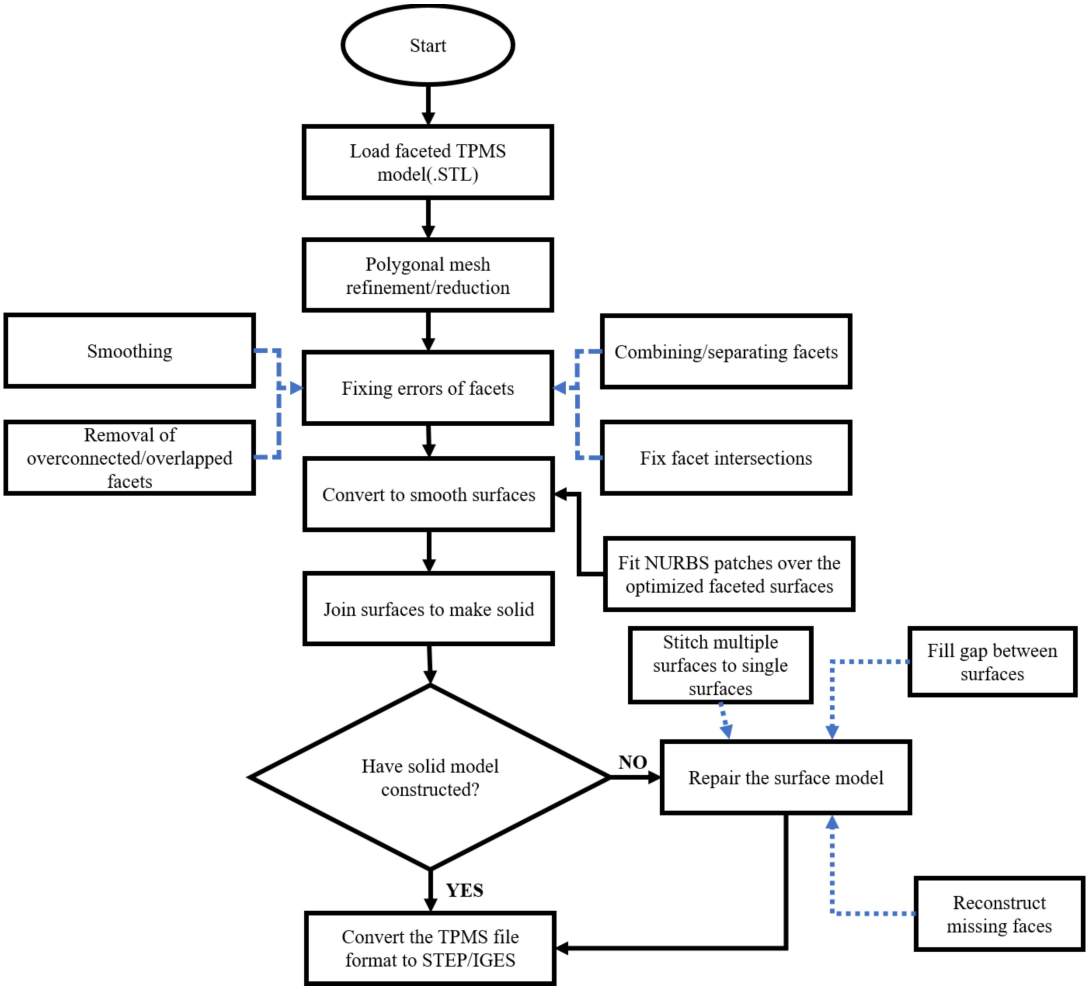

Figure 3.16. Process flow diagram for the conversion of TPMS STL data to multiscale CAD design.

3.8 TPMS Unit cell shape and size identification

The unit cells of several TPMS architectures were developed using the techniques mentioned in previous section. The porosities included in this study range from 50 to 90 % for each structure. Identification of these porosities depends on the literature which clearly shows that between these ranges porous structures purely mimic the cortical and cancellous bone.

The influence of unit cell size was assessed for all TPMS structures by generating unit cells of 1, 2, 3, 4, and 5, respectively. However, the material volume was kept constant. To produce a regular volume of materials and external borders, the strut thickness and pore sizes were regulated. The maximum Von Mises stress on the structure was recorded. The observations led to the conclusion that a minimum unit cell size of 1 mm (Figure 3.17), that will produce a superior mechanical performance, and will have the characteristics of an infinite structure while doing finite element analysis. This details are discussed in the next section along with the lattice size determination. Also, it should be noted that the description of material and boundary conditions for this determination will be discussed in detail in later section of Material and boundary conditions.

However, the unit cell shape was cubic with dimensions of 1×1×1 mm for each unit cell as shown in Figure 3.17. Thickness of the structures "t" is highly dependent on the porosity of each structure which will be discussed in detail in later section.

Additionally, as shown in Figure 3.18, the outcomes of sensitivity analysis of unit cell sizes for a certain porosity indicated that the Von Mises stress increases as the unit cell size decreases. With maximum Von Mises stresses ranging from 1831 to 1792 MPa, 10% porous structures with varying unit cell sizes of 1 to 5 mm were found to have better mechanical performances.

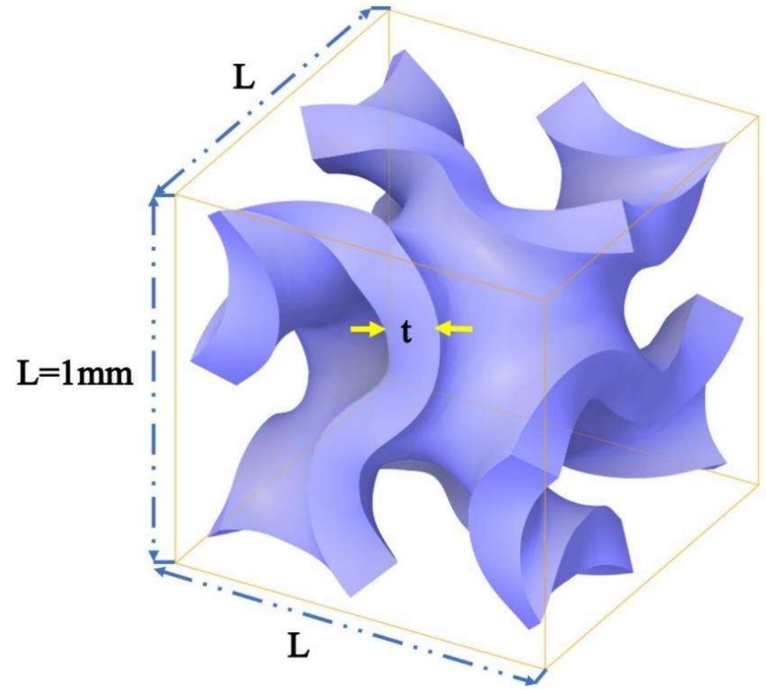

Figure 3.17: Illustration of unit cell shape, size and strut thickness

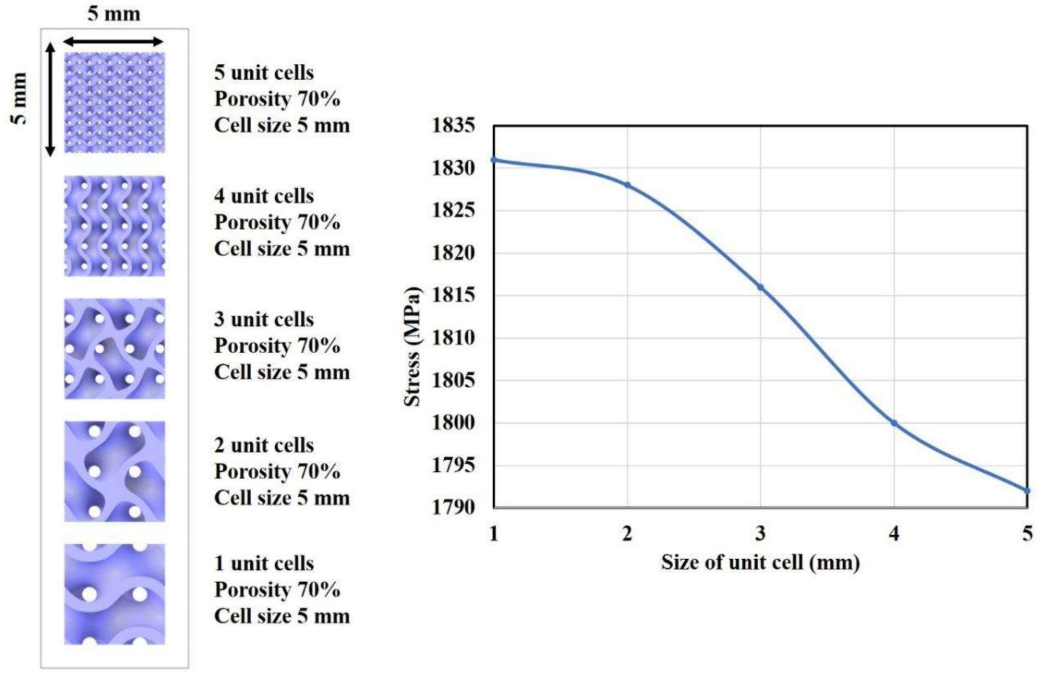

Figure 3.18: Estimation of maximum Von Mises stress of different sizes of unit cells on constant volume fraction and porosity

These were consistent with the findings of Yan C. et al., who scaled the unit cell size from 2 mm to 8 mm and determined the effective Young's modulus between 241.36 MPa and 305.72 MPa (Yan et al. 2012). Although the porosity was set at 70%, the structure was designed with gyroid cells made of 316L stainless steel. However, based on the findings of this investigation, it was decided to continue studying the 1 mm unit cell size because it displayed a nearly consistent behaviour for all five unit cells. As a consequence of the investigation, the results showed that an optimum mechanical property may be obtained while utilising the least number of unit cells.

3.9 Finite number of unit cells in a lattice for finite element studies

Figure 3.19 depicts the replication of 1 to 5 number of unit cells in 3-dimensional space. As shown in Figure 3.20, the porosities and unit cell sizes were maintained during the replication of the unit cells between 1 to 5. To simulate the performance of an infinite model, a finite number of unit cells have been utilized to approximate the mechanical behaviour of the structure. The top and bottom sides were connected to the rigid plates, that were constructed using unit cells of the similar dimensions. However, the material property, compression plate, boundary conditions and mesh sensitivity analysis done for the evaluation of finite number of unit cells in a lattice were same for the whole work and are disused in detail in later section. The FEA was used to compute the effective Young's modulus (Eeff) using Hooke's law. This stage anticipated the smallest number of unit cells that might imitate the required mechanical characteristics of infinite structures. From the Figure 3.20, it can be observed that modulus change for one unit cells is maximum and for two repetitions is minimum.

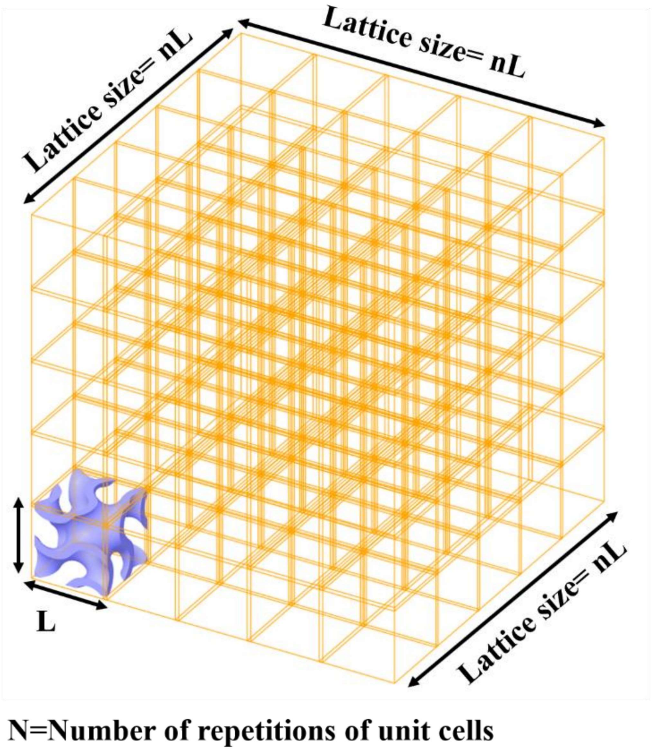

Figure 3.19: Cubical space for the number of unit cell repetitions

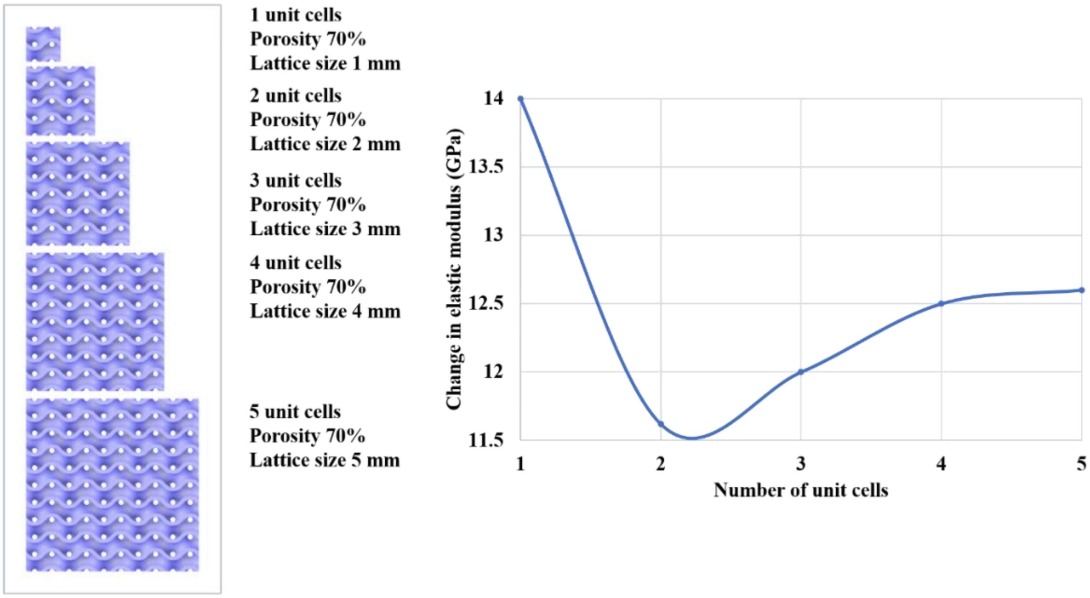

Figure 3.20: The effective Young's modulus of a finite model with a number of unit cells varying from 1 to 5 is predicted.

However, as the number of unit cells increases, there is a slight increase in modulus change but is almost steady after two numbers. To avoid the computational time, two nuber of units cell repetitions were adopted in a lattice in all X,Y and Z coordinate. So, an appropriate lattice size used in this study for finite element analysis is 2×2×2. Quevedo Gonzalez F. J. and Nuno N. concluded that models with a minimum of eight unit cells may accurately anticipate the behaviour of infinite structures (Gonzalez and Nuno 2016). The finite unit cells in the strut-based lattice were also predicted by Hassan Mehboob, who determined that a lattice should have at least four unit cells (Mehboob et al. 2018).

3.10 Unit cell and lattice cell representation for developing PS porous scaffold

The developed solid unit cell structures were periodically patterned with N=2 number of times in X, Y, and Z Cartesian coordinates to obtain a NxNxN structure, which is further used for FEA. Figure 3.21 shows a general representation of unit cell and 2x2x2 TPMS lattice structures to evaluate the morphological and mechanical properties.

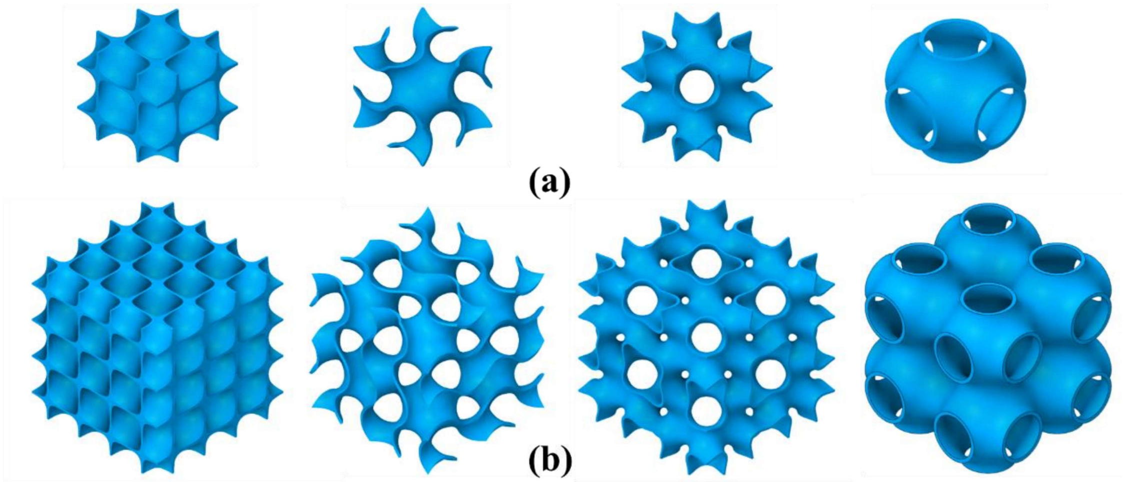

Figure 3.21: General view of typical TPMS models used**:** from left to right D, G, IWP, and P surface, respectively (a) Unit Cell (b) TPMS Lattice Structure.

It is a general representation of all four models for a single porosity of 90%. However, for a single TPMS model, a porosity range from 50% to 90% with an interval of 10% was used to investigate the morphological and mechanical behaviour of these TPMS structures.